Synchronized delta oscillations correlate with the resting-state functional MRI signal

Hanbing Lu*, Yantao Zuo*, Hong Gu*, James A. Waltz†, Wang Zhan*, Clara A. Scholl*, William Rea*, Yihong Yang*‡, and Elliot A. Stein*‡

*Neuroimaging Research Branch, National Institute on Drug Abuse, Intramural Research Program, National Institutes of Health, Baltimore, MD 21224; and †Maryland Psychiatric Research Center, University of Maryland School of Medicine, Baltimore, MD 21201

Edited by Edward G. Jones, University of California, Davis, CA, and approved September 28, 2007 (received for review June 20, 2007)

Synchronized low-frequency spontaneous fluctuations of the functional MRI (fMRI) signal have recently been applied to investigate large-scale neuronal networks of the brain in the absence of specific task instructions. However, the underlying neural mechanisms of these fluctuations remain largely unknown. To this end, electrophysiological recordings and resting-state fMRI measurements were conducted in α-chloralose-anesthetized rats. Using a seed-voxel analysis strategy, region-specific, anesthetic dose-dependent fMRI resting-state functional connectivity was detected in bilateral primary somatosensory cortex (S1FL) of the resting brain. Cortical electroencephalographic signals were also recorded from bilateral S1FL; a visual cortex locus served as a control site. Results demonstrate that, unlike the evoked fMRI response that correlates with power changes in the γ bands, the resting-state fMRI signal correlates with the power coherence in low-frequency bands, particularly the δ band. These data indicate that hemodynamic fMRI signal differentially registers specific electrical oscillatory frequency band activity, suggesting that fMRI may be able to distinguish the ongoing from the evoked activity of the brain.

electroencephalogram | spontaneous fluctuations | functional connectivity

The human brain is thought to be composed of multiple coherent neuronal networks of variable scales that support sensory, motor, and cognitive functions (1). The traditional approach to studying such networks has been to use specific tasks to probe neurobiological responses. In contrast, recent studies have demonstrated the existence of spontaneous, low-frequency (i.e., <0.1 Hz) fluctuations in the functional MRI (fMRI) signal of the resting brain that exhibit coherence patterns within specific neuronal networks in the absence of overt task performance or explicit attentional demands (2–4). Such precisely patterned spontaneous activity has been reported in both awake human and anesthetized nonhuman primates (5). Recently, "resting-state" fMRI has been applied to study alterations in brain networks under such pathological conditions as Alzheimer's disease (6), multiple sclerosis (7), and spatial neglect syndrome (8). These studies collectively suggest that, rather than simple physiological artifacts induced by cardiac pulsations or respiration, as was originally suspected, these widely distributed coherent low-frequency fMRI fluctuations have a direct neural basis (9, 10). However, more than a decade since they were first identified, the linkage between neuronal activity and resting-state fMRI signal remains largely unknown, underscoring the clear and critical need for well controlled animal models to investigate this phenomenon.

Across various states of vigilance, the electrical activity of neuronal networks is known to oscillate at various frequencies and amplitudes, with high-frequency oscillations confined to local networks, whereas large networks are recruited during slow oscillations (11, 12). Imposed tasks alter local field potential (LFP) and neuronal spiking. Accumulating data point toward a tight coupling between the hemodynamic response and LFPs (13, 14). A recent study by Niessing *et al.* (15) further demonstrated that the hemodynamic response to visual stimulation correlates specifically with evoked LFP oscillations in the high γ frequency band. It should be noted that these studies investigated the evoked responses to specific task manipulations, a condition where alterations in high-frequency LFP power are known to be prominent. In contrast, during quiet rest and sleep, changes in high-frequency LFP power are less pronounced (16, 17). These observations led us to investigate the electrophysiological bases of the resting-state fMRI signal.

We present here the results of an electrophysiological and resting-state fMRI study by using a recently developed rat model (18, 19). By using cerebral blood volume-weighted fMRI with a superparamagnetic contrast agent, we achieved enhanced sensitivity and functional specificity (20, 21) and were able to detect region-specific and anesthetic dose-dependent synchronized fMRI fluctuations in the primary somatosensory cortex (S1FL) of the resting rat brain. Epidural electroencephalographic (EEG) signals were recorded from bilateral S1FL electrodes by using the same animal model. Results demonstrate that, unlike the evoked fMRI response that correlates with power changes in high-frequency bands, power coherence in low-frequency bands, particularly the δ band, correlates with the resting-state fMRI signal and does so in a region-specific and dose-dependent fashion. These results add a previously undescribed dimension and insight into the linkage between neuronal activity and hemodynamic response-based fMRI signal.

Results

Anesthetic Dose-Dependent Resting-State Functional Connectivity in Rat S1FL. The synchrony of spontaneous fluctuations within and among brain regions has been traditionally studied by probing the correlation (or anticorrelation) of the resting-state fMRI time course to a seed point of interest, the statistical results of which are used to generate "functional connectivity" maps (2–4). We have taken a similar approach and investigated functional connectivity within and between the rat primary somatosensory cortices. Because anesthetic agents are known to modulate states of consciousness and can be expected to influence the synchrony of neuronal networks (22), we also examined the effects of variable anesthetic levels on functional connectivity by sequentially increasing the dose of α-chloralose. At each dose

Author contributions: H.L. and Y.Z. contributed equally to this work; H.L., Y.Z., W.Z., Y.Y., and E.A.S. designed research; H.L., Y.Z., C.A.S., and W.R. performed research; H.L., Y.Z., H.G., J.A.W., W.Z., C.A.S., and Y.Y. analyzed data; and H.L., Y.Z., H.G., Y.Y., and E.A.S. wrote the paper.

The authors declare no conflict of interest.

This article is a PNAS Direct Submission.

Abbreviations: fMRI, functional MRI; LFP, local field potential; EEG, electroencephalographic; CC, cross-correlation coefficients; S1FL, bilateral primary somatosensory cortex; RV, right visual cortex; LF, left S1FL, RF, right S1FL.

‡To whom correspondence may be addressed. E-mail: yihongyang@intra.nida.nih.gov or estein@intra.nida.nih.gov.

This article contains supporting information online at www.pnas.org/cgi/content/full/0705791104/DC1.

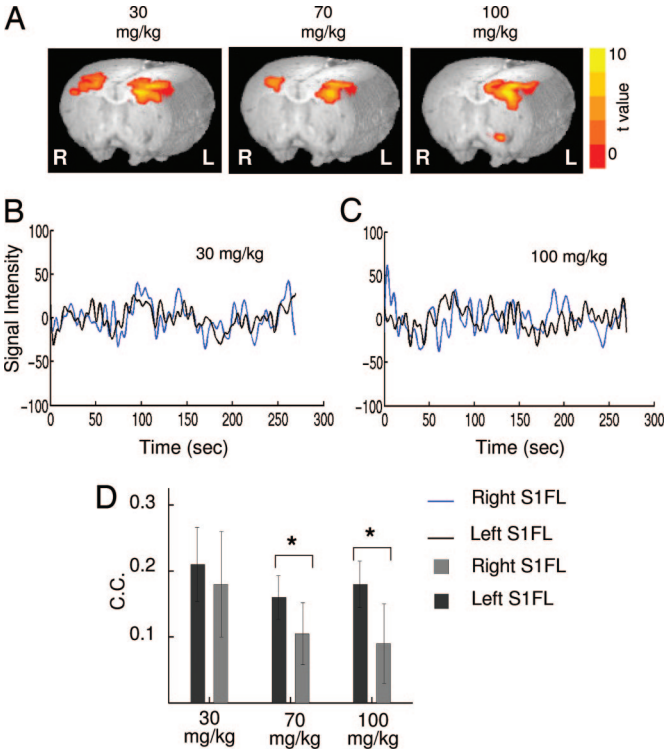

Fig. 1. Effect of α-chloralose dose on resting-state functional connectivity in rat primary somatosensory cortex (S1FL). (*A*) 3D representation of color-coded group *t*-statistical maps thresholded at $P < 0.025$ ($n = 6$). The seed voxels were chosen from the left S1FL. Functional connectivity within the left hemisphere persisted during all three doses of α-chloralose, whereas the functional connectivity within the right hemisphere decreased as the anesthesia dose increased, suggesting that interhemispheric synchrony of the spontaneous fluctuations was significantly modulated by α-chloralose. (*B* and *C*) Low-pass-filtered resting-state fMRI time courses (with mean removed) at α-chloralose dose of 30 and 100 mg/kg from one animal (cutoff frequency = 0.1 Hz). Time courses from bilateral S1FL appear visually to be more synchronized at low anesthesia levels. CC values in bilateral S1FL at three anesthetic doses are shown in *D*. CC values in the right hemisphere were significantly reduced compared with those in the left hemisphere at α-chloralose doses of 70 and 100 mg/kg. There was no significant difference at 30 mg/kg. *, $P < 0.05$.

(30, 70, and 100mg/kg), both resting and evoked fMRI responses to electrical forepaw stimulation were acquired (see *Methods*). We detected robust dose-dependent fMRI signals after electrical forepaw stimulation across all anesthesia levels, with the evoked responses at 100 mg/kg significantly smaller than at the lower two doses [see supporting information (SI) Fig. 6].

Fig. 1*A* shows a 3D representation of group functional connectivity maps superimposed onto T_1-weighted anatomical images. Seed voxels were selected in the left S1FL based upon activation maps derived from electrical forepaw stimulation data (see SI Fig. 6). Functional connectivity was clearly seen in the ipsilateral S1FL at all three α-chloralose doses. In contrast, functional connectivity on the contralateral side decreased as the anesthetic dose increased. No significant interhemispheric connectivity was detected at 100 mg/kg α-chloralose. Fig. 1 *B* and *C* show representative resting-state time courses from bilateral S1FL after α-chloralose doses of 30 and 100 mg/kg, respectively. In general, the spontaneous fluctuations visually appear to be more synchronized at the low dose. Quantitative results are depicted in Fig. 1*D*. The average cross-correlation coefficients (CC) within statistically significant ipsilateral somatosensory voxels were 0.21 ± 0.06, 0.16 ± 0.03, and 0.18 ± 0.04 at α-chloralose doses of 30, 70, and 100 mg/kg, respectively. There

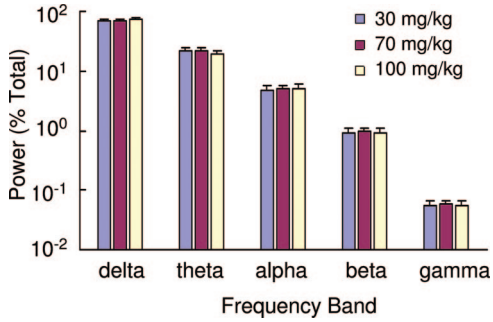

Fig. 2. Semilog plot of the distribution of EEG power across frequency bands in α-chloralose-anesthetized rats. Low frequencies, in particular the δ band, dominate the power spectra. There were no significant differences in the power distributions between the three levels of anesthesia ($n = 8$ rats).

were no significant differences in CCs between these conditions (repeated-measures ANOVA), suggesting that intrahemispheric low-frequency fluctuations remained synchronized across anesthesia levels. In contrast, the average CCs in the contralateral S1FL decreased as a function of dose (0.18 ± 0.08, 0.11 ± 0.05, and 0.09 ± 0.06 at 30, 70, and 100 mg/kg, respectively). Further, there was no significant difference in the averaged CCs between the left and right S1FL at 30 mg/kg α-chloralose (two-tailed paired *t* test), suggesting that interhemispheric low-frequency fluctuations remained highly synchronized. However, at the two higher doses, CC values between the left and right cortices were significantly different ($P < 0.05$). These data suggest that the synchrony of interhemispheric low frequency fluctuations within the S1FL were subject to and modified by anesthetic dose.

Neural Correlates of Resting-State fMRI Signal. Our next step was to explore the neural linkage of the above interhemispheric synchronous fluctuations. Previous studies have demonstrated that evoked EEG and fMRI signals are tightly coupled (23, 24). We have taken a similar approach and have recorded epidural EEG signals from electrodes placed bilaterally over the S1FL in a separate group of animals ($n = 8$). A third electrode was placed over the visual cortex to serve as a control site. The experimental protocol was identical to the above fMRI experiments (see *Methods*). We hypothesized that the underlying electrophysiological signal driving the interhemispheric synchronized spontaneous fluctuations in S1FL should also be anesthetic dose-dependent and should uniquely distinguish it from that between the S1FL and the visual cortex.

EEG power has been used to link electrical activity with blood flow and fMRI signal (25–27). We conducted power spectral density analyses on the resting-state EEG signal within seven predefined frequency bands based on EEG convention (10) (δ, 1–4 Hz; θ, 5–8 Hz; α, 9–14 Hz; β, 15–30 Hz; γ_L, 30–50 Hz; γ_H, 50–100 Hz; and γ_{VH}, 100–150 Hz). At each anesthetic level, the power distribution within each frequency band was normalized to the corresponding total power and averaged across animals. Fig. 2 shows averaged power distributions across anesthetic levels from the right S1FL (EEG power at frequency >50 Hz were not plotted because of very low values). The distributions generally follow the classic 1/f law (28), with the δ and θ bands accounting for 71.8 ± 2.5% and 21.7 ± 1.9% of the total EEG power, respectively. The higher-frequency bands accounted for only ≈6.5% of total EEG energy. There were no significant differences in power distribution among the three electrodes or the three anesthetic levels. These results demonstrate that resting-state EEG signals in α-chloralose-anesthetized rats are dominated by low frequency activity, particularly in the δ and θ bands, whereas the power distribution pattern within individual frequency bands remained unchanged across the anesthetic regime.

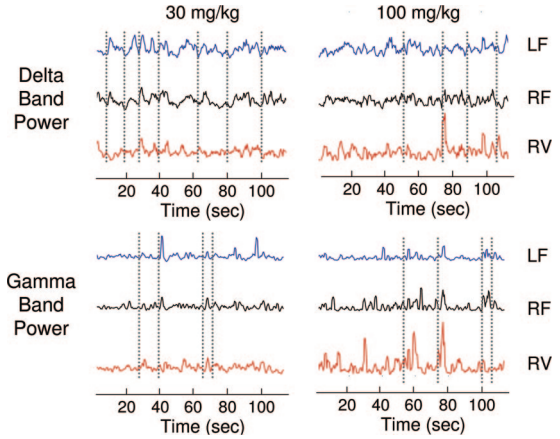

Fig. 3. Power time courses showing variations of the EEG signal from the bilateral S1FL and the visual cortex from one animal. Dotted vertical lines indicate covariations of signals among the three recording sites. δ band power time courses from bilateral S1FL (LF, RF) exhibited more synchronized fluctuations than from right visual cortex (RV), and the synchrony was more pronounced at 30 mg/kg than at 100 mg/kg α-chloralose. Only δ and γ band power time courses are shown for graphic clarity.

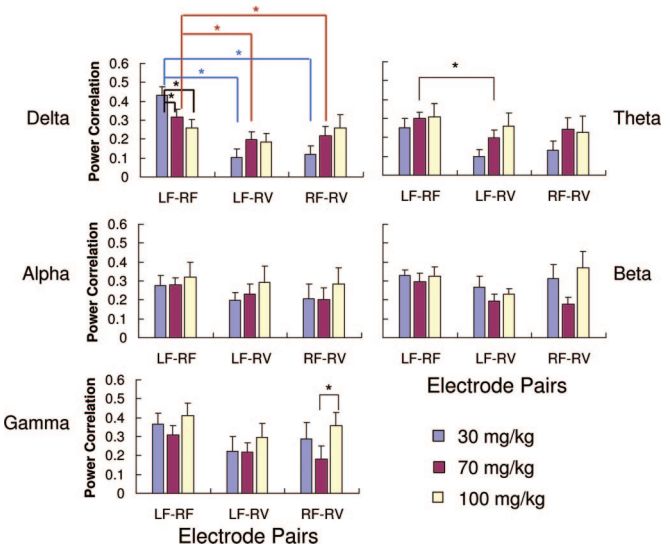

Fig. 4. Statistical comparisons of power correlations between electrode pairs and anesthesia levels. For the δ band, at 30 mg/kg α-chloralose, the power correlation between the left and right somatosensory cortical electrodes was significantly higher than at the two higher doses (Wilcoxon signed-ranks test, $P < 0.04$). No significant dose differences were found for either the LF or the RF electrode and the RV. Among electrode pairs, the differences were most pronounced at 30 mg/kg, where the power correlations between LF-RF electrodes were greater than those between LF-RV and between RF-RV pairs (Wilcoxon signed-ranks test, $P = 0.01$ and 0.02, respectively). *, $P < 0.05$. (Abbreviations as in Fig. 3.)

We then analyzed power correlations of EEG recordings from the left and right S1FL and the visual cortex (see *Methods*). Fig. 3 shows representative power time courses from one animal in the δ and γ bands from the three recording electrodes at two anesthetic levels. For the δ band, the CC between the left S1FL (LF) and right S1FL (RF) was 0.63 at 30 mg/kg of α-chloralose. In contrast, it was 0.11 between the LF and right visual cortex (RV), and 0.26 between the RF and RV. At 100 mg/kg, these correlations changed to 0.49, 0.21, and 0.31, respectively, for the same three electrode pairs. In contrast, for the γ band, these correlations were 0.39, 0.31, and 0.33, respectively, at 30 mg/kg, and they changed to 0.43, 0.37, and 0.44 at 100 mg/kg α-chloralose. These data suggest that the temporal covariation of EEG power between these electrode pairs was modulated by anesthetic depth.

Results of power correlation analyses from all animals ($n = 8$) are summarized in Fig. 4. For the LF and RF, the power in the EEG δ band were both significantly correlated and significantly modulated by anesthetic dose (Friedman test, $P < 0.01$). In contrast, the power correlation between the somatosensory cortices and the visual cortex was generally smaller and did not show anesthetic dose-dependence. At an α-chloralose dose of 30 mg/kg, the power correlation between LF and RF electrodes was significantly higher than at both higher doses (Wilcoxon signed-rank test, $P < 0.04$). Among electrode pairs, the differences were most pronounced at 30 mg/kg, with the power correlation between LF–RF electrodes significantly greater than those between LF-RV (Wilcoxon signed-rank test, $P = 0.01$) or between RF–RV pairs ($P = 0.02$). These results demonstrate that the interhemispheric power correlation between the left and right somatosensory cortices was significantly greater than that between the somatosensory cortex and the visual cortex, and it was significantly modulated by anesthetic dose, suggesting a region-specific and anesthetic induced state-dependent effect. As shown in Fig. 5, there was a very similar anesthetic dose-dependent modulation of the δ band EEG power and the resting-state fMRI signal in bilateral S1FL.

In addition to the above analyses on resting-state EEG data, we also acquired evoked potentials after unilateral electrical forepaw stimulation at each anesthesia level and conducted time-frequency analyses on the evoked EEG data (see *Methods*). SI Fig. 7 shows an evoked EEG signal in one session and the results of time-frequency analysis averaged across eight animals. Consistent with previous studies (13, 15), brief stimulation induced EEG power changes primarily in the high-frequency γ bands. Such power changes have been thought to underlie the neural correlates of the evoked fMRI response.

Discussion

In the present study, we examined the relationship between the resting-state fMRI signal and its underlying neuronal activity. Using a recently developed animal model (18, 19), we detected region-specific resting-state functional connectivity within unilateral and between bilateral S1FL, which was modulated by anesthetic levels. This result is consistent with a recent human study that showed reduced functional connectivity in motor cortices with increased doses of sevoflurane anesthesia (29). We further demonstrated that EEG power correlation in the δ band between the LF and RF was significantly greater than that between the S1FL and a minimally connected site serving as a control region, and it too exhibited significant anesthetic dose dependence. Our data strongly suggest that, unlike the evoked fMRI response that correlates with EEG power changes in

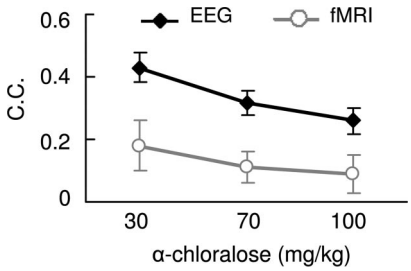

Fig. 5. Anesthetic dose modulations of the δ band EEG power and resting-state fMRI signals in bilateral S1FL. Note the similar patterns of anesthetic dose modulation on these two signal types. C.C. is the cross-correlation coefficient of the EEG power time course and fMRI signal within bilateral S1FL.

high-frequency bands (refs. 13 and 15; SI Fig. 7), power correlations within low-frequency bands, particularly the δ band, underlies the neural correlates of the resting-state functional connectivity.

Resting-state fMRI has recently been applied to study large-scale brain networks. For example, by examining the spontaneous fluctuations of the resting-state fMRI time course, Fox *et al.* (4) identified two brain networks, one of which consists of regions that routinely exhibit task-related activations associated with visual attention, including the inferior parietal lobule and inferior precentral sulcus, whereas the other network was anti-correlated to the above network and included the superior frontal and inferior temporal lobules. From an electrical activity perspective, the spatial and temporal scale of brain oscillatory activity has been well documented (11). In general, the timing and spatial localization of high-frequency oscillations are more specific to the putative timing and localization of brain activation, whereas low-frequency oscillatory activity extends across a larger spatial range (30). Interestingly, from a biophysics perspective, Voss and Clarke (31) observed that a signal's spatial correlation at a given frequency increases as the frequency decreases. Given that resting-state fMRI signals have been proposed to represent synchronous spontaneous fluctuations of large-scale brain networks (3–5), and that long-range synchronized neuronal activity occurs at low frequencies (11), our finding that low-frequency activity, particularly δ band activity, underlies the neural correlates of resting-state fMRI functional connectivity is consistent with this concept.

α-Chloralose has minimal effects on the autonomic, cardiovascular, and cerebral vascular systems (32), and has been the anesthesia of choice in many animal fMRI studies (33). It enhances $GABA_A$ receptor activity (34) and has been thought to temporally and spatially disrupt the negative feedback of the reticulocortico-reticular pathway (32, 35). In this study, we modulated functional connectivity by modulating anesthesia levels and found that interhemispheric functional connectivity between S1FL was significantly modulated by α-chloralose, whereas intrahemispheric low-frequency fluctuations remained synchronized across doses. Epidural EEG recordings revealed that δ band power correlation between bilateral S1FL was modulated in an anesthesia dose-dependent fashion (Figs. 3 and 4), which uniquely distinguished it from the power correlation between the S1FL and the control site (LF–RV or RF–RV). Power correlations in other frequency bands exhibited little or no dose dependency or regional specificity. In a study using a combination of transcranial magnetic stimulation and EEG recordings in human subjects at different conscious states, Massimini *et al.* (36) reported a breakdown of transcallosal and long-range effective connectivity during nonrapid eye-movement sleep, with the evoked electrical responses limited to the stimulus site. In contrast, the evoked response propagated several centimeters away within both ipsi- and contralateral connected areas during quiet wakefulness. Given that anesthetics also modulate the state of consciousness, our finding that interhemispheric functional connectivity between bilateral S1FL was reduced at deeper levels of anesthesia as shown in Fig. 1 is consistent with this human study.

The behavioral significance and physiological functions of the δ rhythm are not well understood. The δ rhythm has been implicated in slow-wave sleep (16) and in supporting normal awake physiological functions (37, 38). For example, Babiloni *et al.* (37) reported that interhemispheric and frontoparietal δ band synchronization is reduced in patients with mild Alzheimer's disease and vascular dementia compared with normal subjects. Animal studies have suggested a role for the δ rhythm in subcortical EEG synchronization (39, 40). For example, Leung *et al.* (39) observed synchronized δ-band activity in bilateral nucleus accumbens of both urethane-anesthetized and freely moving rats, which was suppressed by electrical stimulation of the ventral tegmental area. In the context of neuroimaging, a direct linkage between δ-band activity and fMRI signal in the nucleus accumbens of the rat brain after heroin challenge was reported by Li *et al.* (41).

The mechanisms leading to interhemispheric synchronization of EEG rhythms are under active investigation (42, 43). Cortico-cortical callosal connections appear to play an important role (44, 45). Mice with callosal dysgenesis show a decreased interhemispheric coherence in the δ rhythm during nonrapid eye-movement sleep compared with control strains (46). In line with animal studies, Lowe *et al.* (47) reported that human subjects with callosal agenesis had reduced resting-state functional connectivity in the auditory cortex. In the present study, we observed a reduction in contralateral connectivity with increasing anesthesia depth, while still maintaining ipsilateral synchrony, supporting a role for δ band activity in normal interhemispheric communication.

Technical Considerations and Limitations. Using a simplified linear model, the fMRI signal has been thought of as the convolution of a neuronal input function with a hemodynamic impulse response function. After brief stimulation, EEG power changes occur primarily in the γ band (refs. 13 and 15; SI Fig. 7), the resulting hemodynamic response has a pattern of evoked response that is event-related, although temporally lagged, as shown by Logothetis *et al.* (13). In the present study, because of a number of technical challenges and limitations, we conducted fMRI studies and electrophysiological experiments separately on different groups of animals. As such, we were unable to compute direct correlations between these two types of signals. In addition, we did not measure single or multiunit activity during the experiments, preventing an exhaustive analysis of the relationship between neurophysiological and imaging data. Furthermore, because low-frequency fluctuations are more widely distributed over the cortical surface (10), the choice of the reference electrode site is important. If it is relatively far from the recording electrode, there may have been a bias in the frequency distribution of the recorded EEG signal because common mode rejection will predominantly affect high frequencies. Therefore, our choice of reference electrode site could have potentially biased the EEG measurement toward low-frequency components. Nevertheless, as shown in SI Fig. 7, we were able to detect robust epidural EEG signals, including high-frequency components from S1FL of both hemispheres after electrical forepaw stimulation. In pilot studies, furthermore, we conducted measurements using semimicro-bipolar electrodes; results were very similar. These observations suggest that such potential bias may not have been significant in the present study.

In summary, by using superparamagnetic contrast agent to enhance both the sensitivity and functional specificity of the fMRI signal, we measured resting-state functional connectivity in bilateral S1FL of the rat brain, which was subject to anesthetic dose modulations. We also measured epidural EEG signals from bilateral S1FL and the visual cortex (serving as a control site). Results demonstrated that only the δ band EEG component from bilateral S1FL were modulated in an anesthesia dose-dependent fashion, which uniquely differentiated it from the EEG signal components at other bands as well as the EEG signals from the control site, strongly suggesting that the synchronized δ oscillations region-specifically and anesthesia induced state dependently correlate with the resting-state fMRI signal.

Methods

fMRI experiments were conducted on a 9.4-T horizontal bore scanner (Bruker Medizintechnik, Karlsruhe, Germany). Superparamagnetic contrast agent Ferumoxtran-10 (Advanced Magnetics, Cambridge, MA) was administered (15 mg/kg, i.v.) to

achieve cerebral blood volume contrast to enhance the sensitivity and functional specificity of the fMRI signal (21). Animal preparation was similar to our previous report (20) and was approved by the Animal Care and Use Committee of the National Institute on Drug Abuse, National Institutes of Health. Briefly, rats ($n = 6$) were artificially ventilated under α-chloralose anesthesia. The anesthesia level was systematically modulated by changing α-chloralose doses: animals received a loading dose (80 mg/kg, i.v.), continuous infusion (30 mg/kg) was initiated 30 min after the loading dose. The second (70 mg/kg) and third (100 mg/kg) doses of α-chloralose were administered manually (i.v.), at a time interval of 50 min between injections. Image acquisition was started 15 min after the beginning of the 30 mg/kg continuous infusion, and the 70 and 100 mg/kg bolus injections, respectively. At each anesthesia level, an fMRI experiment with an electrical forepaw stimulation paradigm was conducted by using a single-shot echo planar imaging sequence, followed by three sessions of resting scans. Scan parameters were: field of view = 3.5×3.5 cm^2, matrix size = 64×64, echo time (TE) = 15 ms, retention time = 1,426 ms, seven slices with thickness of 1.5 mm. A total of 270 volumes were collected in 385 s. Data were analyzed by using AFNI (48) with the seed-point analysis strategy (2).

Electrophysiological experiments ($n = 8$) followed a design parallel to the MRI experiments. General animal preparation, including femoral arterial and venous catheterization, and tracheotomy, etc., were identical to those for the MRI experiments. The skull was exposed, and three craniotomies (2.5-mm diameter) were performed. Two were centered at 1.08 mm anterior and 4.0 mm lateral to bregma over the left and right somatosensory cortex, and the third was centered at 7.0 mm posterior, 2.5 mm lateral to bregma over the RV by using a water-cooled drill. Ball-shaped Ag/AgCl recording electrodes (wire diameter, 0.38 mm; ball diameter, 0.76 mm) were stereotaxically placed on the intact dura at the center of each of the three locations while avoiding large blood vessels. Positions were adjusted slightly until robust evoked signals were recorded. A stainless steel screw was positioned ≈5 mm anterior and 2 mm lateral to bregma to serve as reference electrode. This screw was positioned to penetrate the dura at a point approximately equidistant from the recording electrodes placed bilaterally in S1FL. The animal was grounded with an Ag/AgCl electrode placed in the occipital muscle. EEG signals were amplified at a gain of 1,000, band-pass-filtered at 0.3–1,000 Hz, notch-filtered at 60 Hz (A-M Systems, Model 3600, Carlsborg, WA), and digitally sampled at 2,000 Hz (Redshirt Imaging, New Haven, CT). In one animal, EEG signals were band-pass-filtered at 0.3–10 kHz and sampled at 32 kHz. Results were very similar. EEG data were analyzed in MATLAB (MathWorks, Natick, MA) and EEGLAB (49). Power spectral estimation of the resting EEG signal was obtained by using Thomson's multitaper analysis method (50). Complete methodological details are described in *SI Text*.

We thank Dr. T. J. Ross (National Institute on Drug Abuse) for helpful discussions. Ferumoxtran-10 was kindly provided by Advanced Magnetics, Inc. This work was supported by the Intramural Research Program of the National Institute on Drug Abuse, National Institutes of Health.

1. Buzsaki G, Draguhn A (2004) *Science* 304:1926–1929.
2. Biswal B, Yetkin FZ, Haughton VM, Hyde JS (1995) *Magn Reson Med* 34:537–541.
3. Greicius MD, Krasnow B, Reiss AL, Menon V (2003) *Proc Natl Acad Sci USA* 100:253–258.
4. Fox MD, Snyder AZ, Vincent JL, Corbetta M, Van Essen DC, Raichle ME (2005) *Proc Natl Acad Sci USA* 102:9673–9678.
5. Vincent JL, Patel GH, Fox MD, Snyder AZ, Baker JT, Van Essen DC, Zempel JM, Snyder LH, Corbetta M, Raichle ME (2007) *Nature* 447:83–86.
6. Li SJ, Li Z, Wu G, Zhang MJ, Franczak M, Antuono PG (2002) *Radiology* 225:253–259.
7. Lowe MJ, Phillips MD, Lurito JT, Mattson D, Dzemidzic M, Mathews VP (2002) *Radiology* 224:184–192.
8. He BJ, Snyder AZ, Vincent JL, Epstein A, Shulman GL, Corbetta M (2007) *Neuron* 53:905–918.
9. Vern BA, Schuette WH, Leheta B, Juel VC, Radulovacki M (1988) *J Cereb Blood Flow Metab* 8:215–226.
10. Leopold DA, Murayama Y, Logothetis NK (2003) *Cereb Cortex* 13:422–433.
11. Silberstein RB (2006) in *Event-Related Dynamics of Brain Oscillations*, *Progress in Brain Res*, eds Neuper C, Klimesch W (Elsevier, Boston), pp 63–76.
12. Von Stein A, Sarnthein J (2000) *Int J Psychophysiol* 38:301–313.
13. Logothetis NK, Pauls J, Augath M, Trinath T, Oeltermann A (2001) *Nature* 412:150–157.
14. Lauritzen M, Gold L (2003) *J Neurosci* 23:3972–3980.
15. Niessing J, Ebisch B, Schmidt KE, Niessing M, Singer W, Galuske RA (2005) *Science* 309:948–951.
16. Steriade M (2000) *Neuroscience* 101:243–276.
17. Lopes da Silva FH (2006) in *Event-Related Dynamics of Brain Oscillations*, *Progress in Brain Res*, eds Neuper C, Klimesch W (Elsevier, Boston), pp 3–17.
18. Lu H, Gitajn L, Rea W, Stein EA, Yang Y (2006) *Proc Intl Soc Magn Reson Med* 14:532.
19. Lu H, Gu H, Zuo Y, Scholl CA, Stein EA, Yang Y (2007) *Proc Intl Soc Magn Reson Med* 15:3212.
20. Lu H, Patel S, Luo F, Li SJ, Hillard CJ, Ward BD, Hyde JS (2004) *Magn Reson Med* 52:1060–1068.
21. Mandeville JB, Marota JJ, Kosofsky BE, Keltner JR, Weissleder R, Rosen BR, Weisskoff RM (1998) *Magn Reson Med* 39:615–624.
22. Hudetz AG, Wood JD, Kampine JP (2003) *Anesthesiology* 99:1125–1131.
23. Brinker G, Bock C, Busch E, Krep H, Hossmann KA, Hoehn-Berlage M (1999) *Magn Reson Med* 41:469–473.
24. Ogawa S, Lee TM, Stepnoski R, Chen W, Zhu XH, Ugurbil K (2000) *Proc Natl Acad Sci USA* 97:11026–11031.
25. Buchsbaum MS, Kessler R, King A, Johnson J, Cappelletti J (1984) *Prog Brain Res* 62:263–269.
26. Goldman RI, Stern JM, Engel J, Jr, Cohen MS (2002) *NeuroReport* 13:2487–2492.
27. Laufs H, Kleinschmidt A, Beyerle A, Eger E, Salek-Haddadi A, Preibisch C, Krakow K (2003) *NeuroImage* 19:1463–1476.
28. Bak P, Tang C, Wiesenfeld K (1987) *Phys Rev Lett* 59:381–384.
29. Peltier SJ, Kerssens C, Hamann SB, Sebel PS, Byas-Smith M, Hu X (2005) *NeuroReport* 16:285–288.
30. Crone NE (2000) *Adv Neurol* 84:343–351.
31. Voss RF, Clarke J (1976) *Phys Rev B* 13:556–573.
32. Balis GU, Monroe RR (1964) *Psychopharmacology* 61:1–30.
33. Hyder F, Behar KL, Martin MA, Blamire AM, Shulman RG (1994) *J Cereb Blood Flow Metab* 14:649–655.
34. Garrett KM, Gan J (1998) *J Pharmacol Exp* 285:680–686.
35. Amzica F, Steriade M (1998) *Electroencephalogr Clin Neurophysiol* 107:69–83.
36. Massimini M, Ferrarelli F, Huber R, Esser SK, Singh H, Tononi G (2005) *Science* 309:2228–2232.
37. Babiloni C, Frisoni G, Steriade M, Bresciani L, Binetti G, Del Percio C, Geroldi C, Miniussi C, Nobili F, Rodriguez G, *et al.* (2004) *Eur J Neurosci* 19:2583–2590.
38. Fernandez A, Arrazola J, Maestu F, Amo C, Gil-Gregorio P, Wienbruch C, Ortiz T (2003) *Am J Neuroradiol* 24:481–487.
39. Leung LS, Yim CY (1993) *Can J Physiol Pharmacol* 71:311–320.
40. Goto Y, O'Donnell P (2001) *J Neurosci* 21:4498–4504.
41. Li S-J, Luo F, Schulte M, Hudetz (2006) *Proc Intl Soc Magn Reson Med* 14:797.
42. Singer W (1994) *Int Rev Neurobiol* 37:153–183.
43. Contreras D, Steriade M (1997) *Neuroscience* 76:11–24.
44. Engel AK, Konig P, Kreiter AK, Singer W (1991) *Science* 252:1177–1179.
45. Kiper DC, Knyazeva MG, Tettoni L, Innocenti GM (1999) *J Neurophysiol* 82:3082–3094.
46. Vyazovskiy V, Achermann P, Borbely AA, Tobler I (2004) *Neuroscience* 124:481–488.
47. Lowe MJ, Rutecki P, Turski P, Woodard A, Sorenson J (1997) *NeuroImage* 5:S194.
48. Cox RW (1996) *Comput Biomed Res* 29:162–173.
49. Jung TP, Makeig S, Westerfield M, Townsend J, Courchesne E, Sejnowski TJ (2001) *Hum Brain Mapp* 14:166–185.
50. Imas OA, Ropella KM, Wood JD, Hudetz AG (2004) *Neuroscience* 123:269–278.